



Experimental research on the mechanical properties and energy transfer of fractured granite under triaxial loading

Yi Luo^{1,3} · Kun Xu² · Hangli Gong^{1,2,3} · Dengxing Qu^{1,3,4} · Xinping Li^{1,3} · Gang Wang⁵ · Qiaoliang Li²

Received: 21 April 2021 / Accepted: 25 March 2022 / Published online: 2 April 2022
© Springer-Verlag GmbH Germany, part of Springer Nature 2022

Abstract

The original rock taken from underground powerhouses of Shuangjiangkou Hydropower Station in south-west China was employed to prepare granite samples containing fractures with different dip angles, widths, and lengths. On this basis, the failure process of rock samples with different shapes of fractures under triaxial loading was investigated; furthermore, the mechanical properties, failure mode, and energy transfer of fractured granite under triaxial loading were revealed. The results showed that a significant post-peak stress drop occurs, and the stress then slowly decreases in the form of repeated drops and increases under triaxial compression. The larger the fracture width, the greater the stress drop; with increasing fracture length, the peak stress decreases and the stress varies from slow, fluctuating reduction to abrupt reduction in the post-peak stage. The failure angle of fractured granite grows with the increase of the confining pressure; as the fracture length increases, X-shaped shear failure mode is gradually prominent and the pre-fabricated fractures more significantly dominate the failure mode; at the dip angle within 0 to 60°, the samples are mainly subjected to X-shaped shear failure. The energy storage limit of fractured granite linearly increases with the increase of the confining pressure while linearly decreases with the increase of the fracture length, and it first decreases, and then increases with increasing fracture dip angle.

Keywords Fractured granite · Triaxial loading · Mechanical properties · Failure mode · Energy transfer

Introduction

Numerous microscopic or macroscopic defects (such as joint fractures) in rock further evolve and aggravate under high geostress at depth, which directly influences the stability of rock structures. The mechanical properties and deformation characteristics of fractured rock are mainly affected by the loading state, joint type, and environment. Energy transfer

accompanies the whole process from elastic deformation to initiation, propagation, and coalescence of microcracks until failure of fractured rock. Therefore, it is important to reveal the internal failure mechanism and propagation and evolution process of cracks in fractured rock from perspectives of mechanical properties and the trend in energy transfer.

At present, the evolution of fractures in jointed rock is mainly explored by using theoretical methods, laboratory testing, and numerical simulation. Many scholars in the world have investigated the evolution law of fractures in rock based on the theoretical method (Luo et al. 2020; Yang et al. 2020; Wang et al. 2020a, 2020c). For example, the elastic stress–strain relationship in fractured rock reflects the weakening and anisotropy of mechanical properties of rock based on strain-energy theory (Wu et al. 2020a; Zhang and Valliappan 1990); Zheng et al. (2019) evaluated the effect of discontinuity angle on the mechanical properties of rock samples under triaxial test; meanwhile, they found and modified the deficiency of Yeager's single discontinuity criterion combined with the test data. Some have theoretically surveyed the mode II fracture toughness of rock based on the modified criterion on the average strain

✉ Dengxing Qu
dengxingqu@whut.edu.cn

¹ Hubei Key Laboratory of Roadway Bridge and Structure Engineering, Wuhan University of Technology, Wuhan 430070, China

² School of Civil Engineering and Architecture, Wuhan University of Technology, Wuhan 430070, China

³ Sanya Science and Education Innovation Park, Wuhan University of Technology, Sanya 572024, China

⁴ School of Safety Science and Emergency Management, Wuhan University of Technology, Wuhan 430070, China

⁵ School of Civil Engineering, Shaoxing University, Shaoxing 312000, China

energy density at the crack tip and derived a coalescence model for rock containing multiple fractures (Rashidi et al. 2018; Zhang et al. 2020; Li et al. 2005). Similarly, some scholars analyzed the evolution of fractures in jointed rock through laboratory tests. Brown (1949) conducted the triaxial tests to determine the influences of the geometric features of fractures on the evolution of mechanical properties, deformation, and fractures in rock. By performing uniaxial compression tests on rock samples with pre-fabricated fractures, the crack propagation and failure mechanism of fractured rock have been extensively studied (Bobet and Einstein 1998; Yang et al. 2015; Zhang et al. 2021; Patricia et al. 2016); Gupta et al. (2015) and Liu (2019) proposed the use of a modified criterion on the maximum circumferential stress and further verified the role of T stress in predicting stability of fracture paths and fracture strength of materials. Based on the result of the acoustic emission source location, they found that high-energy fracture points, low-energy small fracture zones, extensive fracture zones, and macroscopic fracture belts gradually develop during the fracturing of rock (Du et al. 2020; Yang et al. 2021); some scholars proposed the criterion of the strain energy density and proposed that defining the uniaxial tensile-compressive stress and biaxial compressive stress can help to predict the fracture and propagation of cracks in rock (Mahmoud et al. 2020; Justo and Castro 2021). Due to the limitations of theoretical methods and laboratory tests, Wu et al. (2020b) explored influences of the joint distribution, joint continuity, and normal stress on the shear behavior of rock and revealed the evolution of cracks in jointed rock by numerical simulations.

Energy loss generally occurs during the evolution of fractures in rock. From the perspective of the energy loss, research into the evolution of fractures in jointed rock is of great significance. By conducting the triaxial unloading test on fine-grained marble, some have suggested that the energy changes in three stages (i.e., energy accumulation, dissipation, and release) during the unloading test and studied the energy dissipation during the failure of rock samples upon unloading of the confining pressure unloading (Wang et al. 2020d; Zeng et al. 2019; Zhu et al. 2011); through investigation of the anisotropic fracture and energy dissipation characteristics of marble under multi-level cyclic loading, they found that the fatigue deformation, strength, and dissipated energy of rock are greatly influenced by cyclic loading (Zhou et al. 2020; Wang et al. 2020b); Mishra and Basu (2012) and Li et al. (2012) conducted uniaxial fatigue loading test with increasing amplitude and three-dimensional (3-d) CT scanning test on granite and marble with multiple defects; some scholars relied on 1.0-Hz frequency cyclic triaxial test results and investigated the mechanical behavior of artificial jointed rock samples with different joint dip

angles under different stress amplitudes and different confining pressures, defining two new damage variables (density) method and residual strain data to describe jointed rock in the three stages of fatigue damage under circulating load (Zheng et al. 2020; Liu and Liu 2017); some analyzed the energy dissipation and energy release characteristics.

Numerous microscopic or macroscopic defects (such as joint fractures) in rock further evolve and aggravate under high geostress in deep parts, which directly influences the stability of rock structures. The mechanical properties and deformation characteristics of fractured rock are mainly affected by the loading state, joint type, and environment. Energy transfer keeps in company with the whole process from elastic deformation to initiation, propagation, and coalescence of microcracks until failure of fractured rock. Therefore, it is significant to reveal the internal failure mechanism and propagation and evolution process of cracks in fractured rock from perspectives of mechanical properties and the law of energy transfer.

Triaxial loading tests on fractured granite

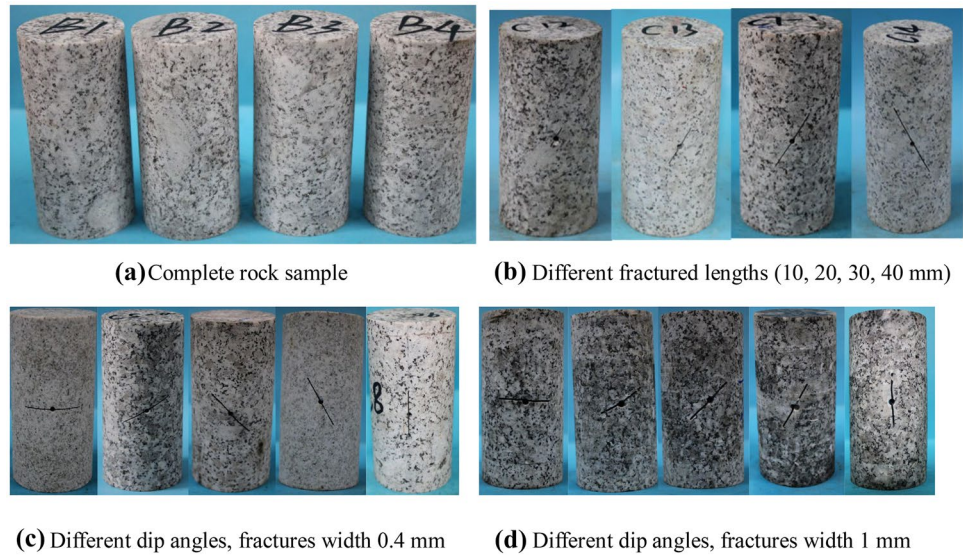
Sample preparation

The original rock (largely intact, with few natural fractures) was sampled from the underground powerhouses of Shuangjiangkou Hydropower Station. In terms of the lithology, the rock mainly appeared as porphyritic biotite moyite, which was processed to form cylindrical rock samples with the diameter of 50 mm and the height-diameter ratio of 2:1 after being core-cut, trimmed, and ground. To reduce the error caused by defects in the specimens themselves, the intact rock samples with relatively approximated longitudinal wave velocity and density were selected to fabricate fractures; the intact samples were drilled through at their centers; thereafter, the samples were cut to form pre-fabricated fractures with widths of 0.4 and 1 mm, respectively; furthermore, the fractured samples with different dip angles (0°, 30°, 45°, 60°, and 90°) and lengths (10, 20, 30, and 40 mm) were prepared (Fig. 1).

Loading schemes and test conditions

The underground powerhouses of Shuangjiangkou Hydropower Station lie at an average burial depth of about 400 m and a maximum geostress of about 37.82 MPa. Based on different shapes (involving length, dip angle, and width) of fractures, the failure mode and trend in energy transfer in rock with different shapes of fractures during triaxial loading under different confining pressures were explored. The working conditions are summarized in Table 1.

Fig. 1 Test specimens. **a** Complete rock sample. **b** Different fractured lengths (10, 20, 30, 40 mm). **c** Different dip angles, fracture width 0.4 mm. **d** Different dip angles, fracture width 1 mm



The mechanical properties of fractured rock were explored based on the pseudo-triaxial test system for rock shown in Fig. 2. During the test, the confining pressure was laterally applied to the pre-set value at the rate of 0.05 MPa/s and the displacement load was axially applied at the rate of 0.002 mm/s. Load was applied until samples were damaged; finally, the stress–strain relationships, strength characteristics, energy transfer, and failure modes of granite samples with different shapes of fractures were determined.

Mechanical properties of fractured granite under triaxial loading

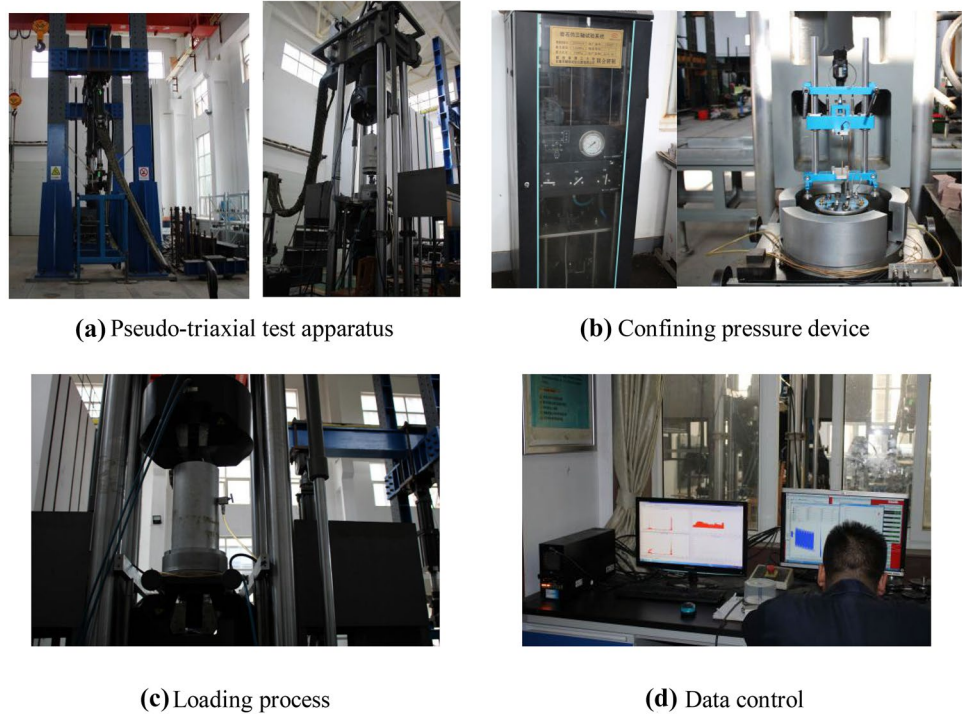
Analysis of the stress–strain curves of fractured granite

1. The influence of confining pressure
 When the dip angle and length of fractures are set to 60° and 30 mm respectively, the stress–strain curves under uniaxial compression and triaxial compression

Table 1 Design of test conditions

Confining pressure (MPa)	Fractured lengths (mm)	Fractures widths (mm)	Fracture dip angle (°)	Diameter (mm)	Height (mm)	Density (kg·m ⁻³)	Weight (g)	Longitudinal wave velocity (cm/s)
40	30	0.40	0	50.26	99.89	508.3	2564.86	4089
40	30	0.40	30	49.96	99.85	507.2	2591.18	4065
40	30	0.40	45	50.22	100.03	508.4	2565.86	3966
40	10	0.40	60	49.97	100.14	507.4	2583.66	4025
40	20	0.40	60	49.78	99.78	508.1	2616.41	4133
40	40	0.40	60	50.30	99.97	507.4	2554.20	3952
0	30	0.40	60	49.76	99.93	509.60	2622.31	4012
20	30	0.40	60	49.68	99.84	508.10	2625.38	4125
40	30	0.40	60	49.83	99.78	507.80	2609.62	4033
60	30	0.40	60	50.12	100.02	508.90	2578.90	4102
40	30	0.40	90	50.14	100.06	509.4	2578.34	3923
40	30	1.00	0	49.86	100.09	507.5	2596.88	3962
40	30	1.00	30	49.74	99.75	507.1	2616.25	3922
40	30	1.00	45	49.93	99.92	508.8	2600.65	3987
40	30	1.00	60	50.06	100.01	508.2	2581.78	4094
40	30	1.00	90	50.14	99.96	509.0	2578.89	4014

Fig. 2 Pseudo-triaxial test system. **a** Pseudo-triaxial test apparatus. **b** Confining pressure device. **c** Loading process. **d** Data control



with different confining pressures are plotted, as shown in Fig. 3. Relative to the radial stress–strain curve, the axial stress–strain curve changes more slowly; as the confining pressure increases, the pre-peak deformation stage is prolonged and the peak stress increases. This indicates that confining pressure increases the peak strength of fractured rock; as the loading continues to the post-peak stage, the stress–strain curve of fractured granite under uniaxial compression exhibits a remarkable difference with that under triaxial compression. To

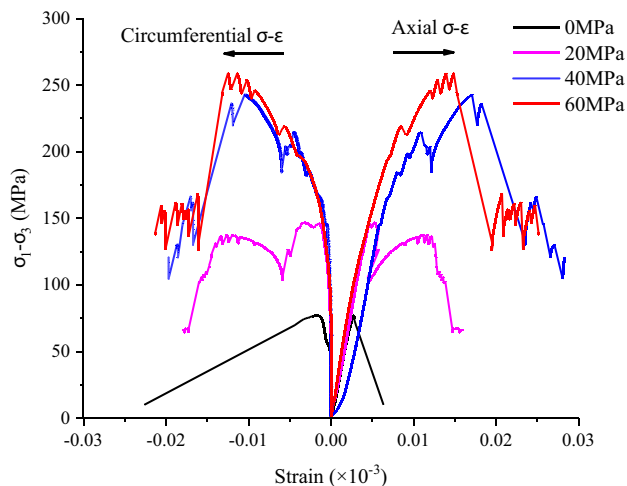


Fig. 3 Stress–strain curves of fractured granite under triaxial loading with different confining pressures

be specific, the curve smoothly decreases in the post-peak stage under uniaxial compression; by contrast, the significant stress drop appears after reaching the peak, and then, the stress slowly decreases in the fluctuating form of repeated drop and increase under triaxial compression. The reason is that the lateral deformation of rock is controlled under the effect of confining pressure. Under uniaxial compression, a large amount of energy is accumulated in rock samples and the testing machine, and after sudden post-peak release of energy, cracks in rock samples converge to form macroscopic fractures. Each stress drop is regarded as the response to coalescence of cracks in rock samples.

2. The influence of fracture length

When keeping the fracture dip angle at 60° and the confining pressure at 40 MPa, the stress–strain curves of rock samples with different fracture lengths under triaxial compression were obtained, as shown in Fig. 4. The data in the figure indicate that the fracture length exerts remarkably different influences on mechanical properties of rock. With the growth of the fracture length, the peak stress gradually declines; the stress–strain curve gradually fluctuates, and the reduction in stress varies from a slow, fluctuating trend to a drastic, sudden one in the post-peak stage. Similarly, the axial strain is much greater than the circumferential strain in granite samples with the same fracture length when

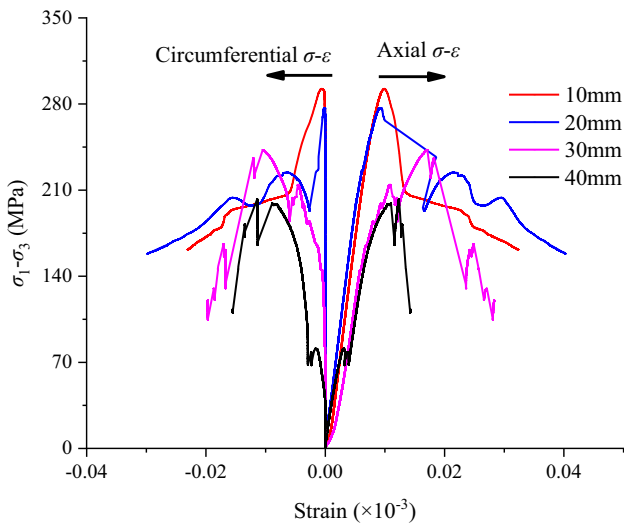


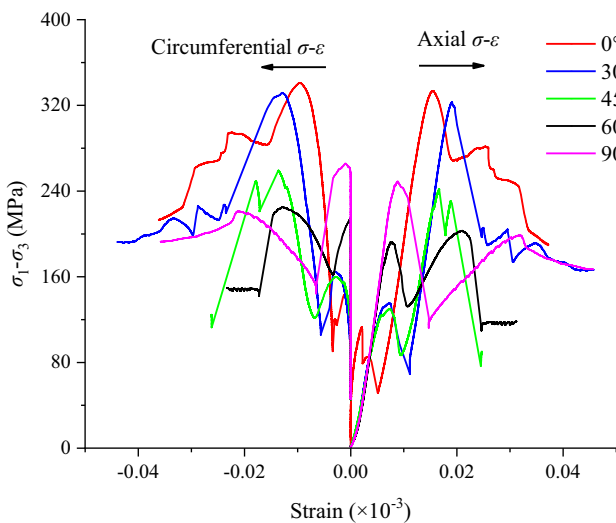
Fig. 4 Stress–strain curves of granite with different crack lengths under triaxial loading

reaching the stress peak; in addition, the samples are not significantly radially deformed under the effect of confining pressure when the fracture length does not exceed 20 mm.

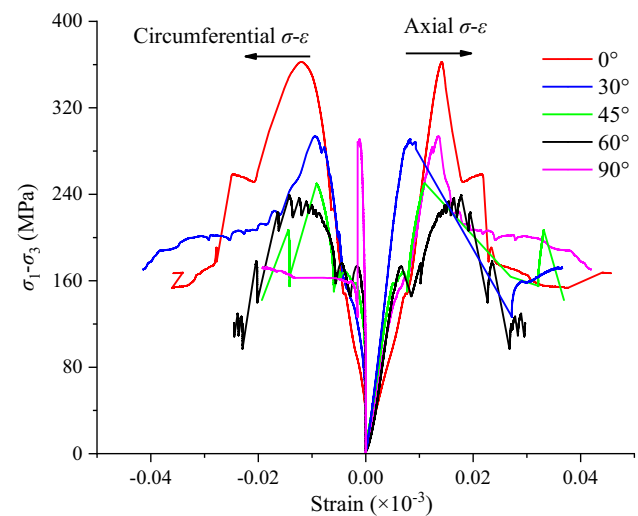
3. The influence of the fracture dip angle

When the fracture length is 30 mm at a confining pressure of 40 MPa, the stress–strain curves of granite samples with the fracture widths of 0.4 and 1 mm at five different fracture dip angles under triaxial loading are as displayed in Fig. 5.

It can be seen from the figure that the fracture dip angle does not alter the trend in the stress–strain curves of rock samples; moreover, the stress–strain curves of rock with different fracture widths present similar behavior and the slopes of the rising curve of rock with different fracture dip angles in the pre-peak stage are generally equivalent; with the increasing fracture dip angle, the peak stresses of granite with different fracture widths first decrease, and then increase. The greatest stress drop occurs in the pre-peak stage of the stress–strain curves of samples with the fracture dip angle of 0 to 60° because wing cracks or wing cracks in the opposite direction (hereinafter referred to as opposite-wing cracks) are generated before the closure of pre-fabricated fractures. During loading, the fractured rock undergoes a compaction stage, an elastic deformation stage, a stable crack propagation stage, an accelerated crack propagation stage, and a post-peak stage. In the initial loading stage, the primary microfractures and pre-fabricated fracture surfaces in rock samples are compressed, closed, and compacted, resulting in the rapid growth of the axial strain; however, the circumferential strain increases due to the effect of the confining pressure. The loading continues until the joint fractures are completely closed. In this case, the rock samples enter the elastic deformation stage, during which the radial deformation increases less relative to the axial strain; as the loading proceeds, the rock samples are in the stable crack propagation stage: the stress–strain curve remains quasi-linear while its slope slightly decreases compared to the elastic stage. The lower the fracture dip angle, the more significant the change. In this stage, the



(a) Fracture width of 1.0 mm



(b) Fracture width of 0.4 mm

Fig. 5 Stress–strain curves of granite with different fracture angles under triaxial loading. **a** Fracture width of 1.0 mm. **b** Fracture width of 0.4 mm

radial strain increases by more than that in the elastic stage; as the load is increased, rock samples reach the rapid crack propagation stage: microcracks in rock samples propagate and converge to evolve into macroscopic fractures; finally, the rock samples are loaded to the post-peak stage. In this stage, the stress–strain curve slowly drops and gradually stabilizes until the samples are completely damaged.

Figure 6 shows the stress–strain curves of granites with different fracture widths (dip angles of 0° and 60°) during triaxial loading under the constant confining pressure (40 MPa) to characterize the change of mechanical properties of granites with different fracture widths under triaxial loading: at the same fracture dip angle, the peak stress decreases with increasing fracture width and the slopes of the curves of rock samples with the two fracture widths in the pre-peak stage are similar. This implies that the fracture width does not significantly affect the elastic modulus of fractured rock; after reaching the stress peak, the stress–strain curve of rock samples with the fracture width of 1 mm fluctuates more than that with a fracture width of 0.4 mm: the wider the fracture, the greater the stress drop.

Analysis of strength parameters of fractured granite

1. The influence of the confining pressure

When the fractures have a length of 30 mm and a dip angle of 60° , the changes in peak strength and elastic modulus of fractured granite during triaxial loading under different confining pressures are illustrated in Fig. 7: the peak strength increases linearly with the

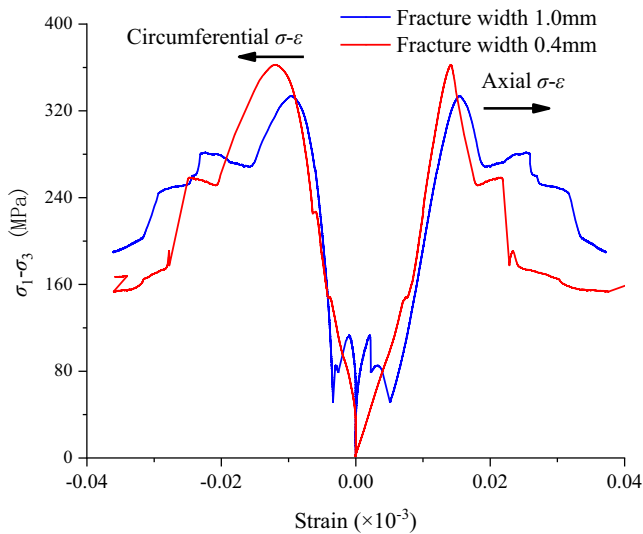
confining pressure; moreover, the peak strength under triaxial compression is greatly higher than that under uniaxial compression. This indicates that the confining pressure can increase the peak strength of fractured rock; the elastic modulus of granite samples containing fractures varies with increasing confining pressure, implying that the change of the confining pressure shows marginal influence on the elastic modulus of fractured rock.

2. The influence of the fracture length

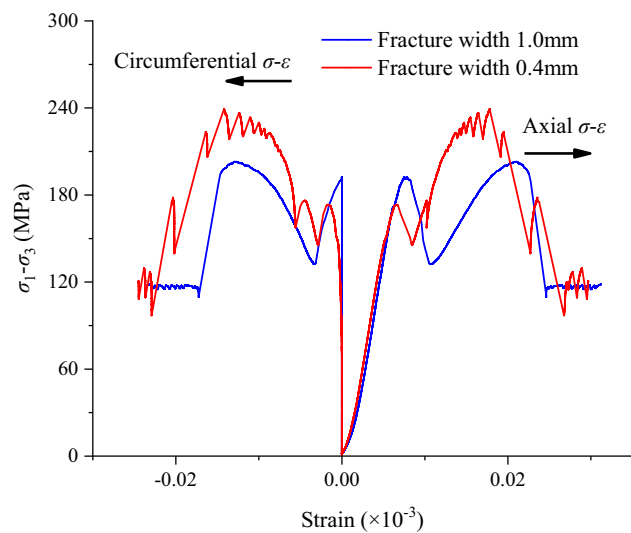
At a fracture dip angle of 60° , Fig. 8 shows the changes in peak strength and elastic modulus of granite with different fracture lengths during triaxial loading under the same confining pressure (40 MPa). As shown in the figure, the peak strength decreases linearly with the increase of the fracture length; at fracture lengths between 10 and 20 mm, both the elastic modulus and deformation modulus increase slightly, which is probably attributed to a certain difference among samples. Overall, the changes in peak strength are similar to those of the elastic modulus: the two parameters both decrease with increasing fracture length: the pre-fabricated fractures reduce the tensile strength and compressive strength of rock.

3. The influence of the fracture dip angle

When the fracture length and the confining pressure are separately 30 mm and 40 MPa, the change curves of the peak strength and elastic modulus of granite samples with different fracture dip angles under triaxial compression are shown in Fig. 9.



(a) A dip angle of 0°



(b) A dip angle of 60°

Fig. 6 Stress–strain curves of fractured granite with different widths under triaxial load. **a** A dip angle of 0° . **b** A dip angle of 60°

Fig. 7 Strength curve of fractured granite under triaxial loading under different confining pressures

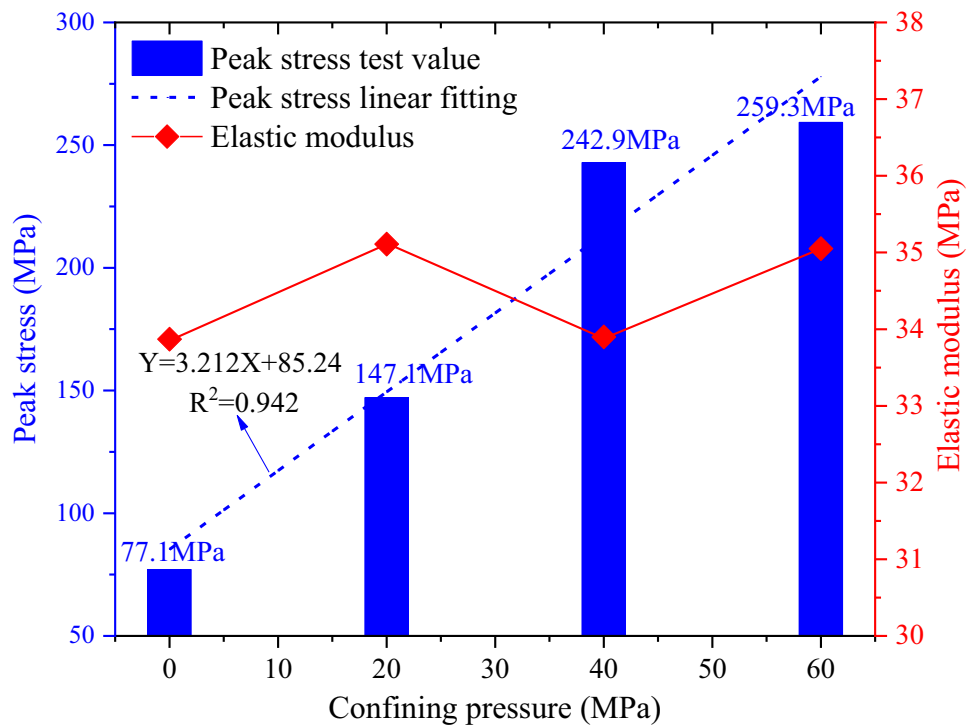
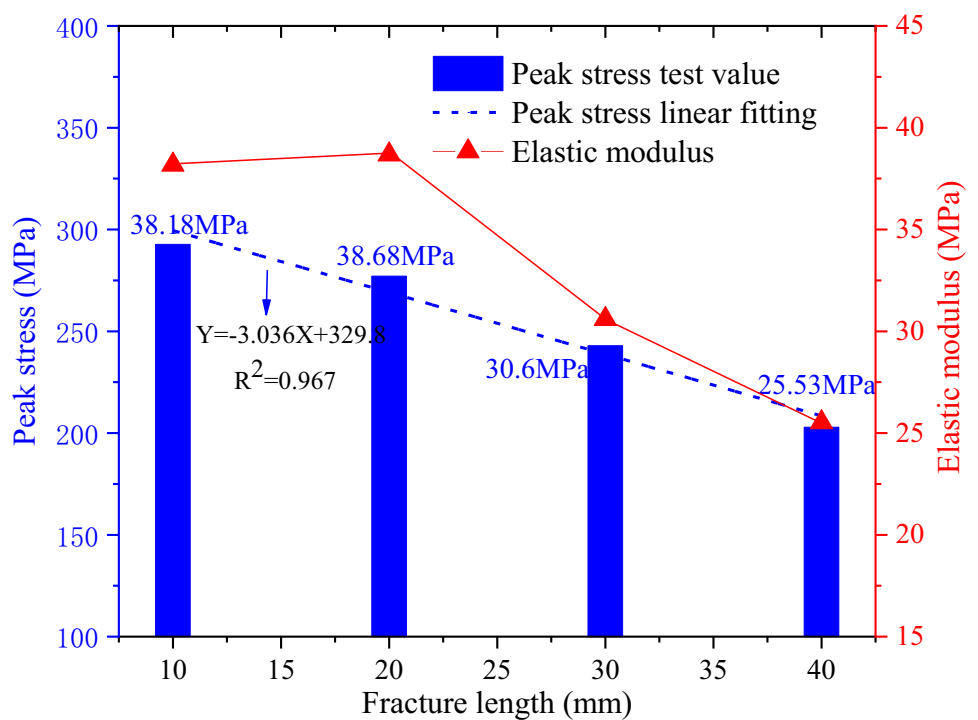


Figure 9 shows that the change in the peak strength with the dip angle generally coincides with that of the elastic modulus of granite samples with different fracture widths. As the fracture dip angle varies, both the peak strength and elastic modulus first decrease, and then increase; this is because with increasing dip angle of pre-fabricated

fractures, shear slip is more likely to occur at the end of fractures under the loading effect, thus decreasing the compressive strength. On condition that fractures develop along the horizontal direction (dip angle of 0°), the peak strengths of rock samples with the fracture widths of 0.4 and 1 mm are up to 362.7 and 333.9 MPa at most; at a fracture dip angle

Fig. 8 Strength curve of granite with different fracture lengths under triaxial loading



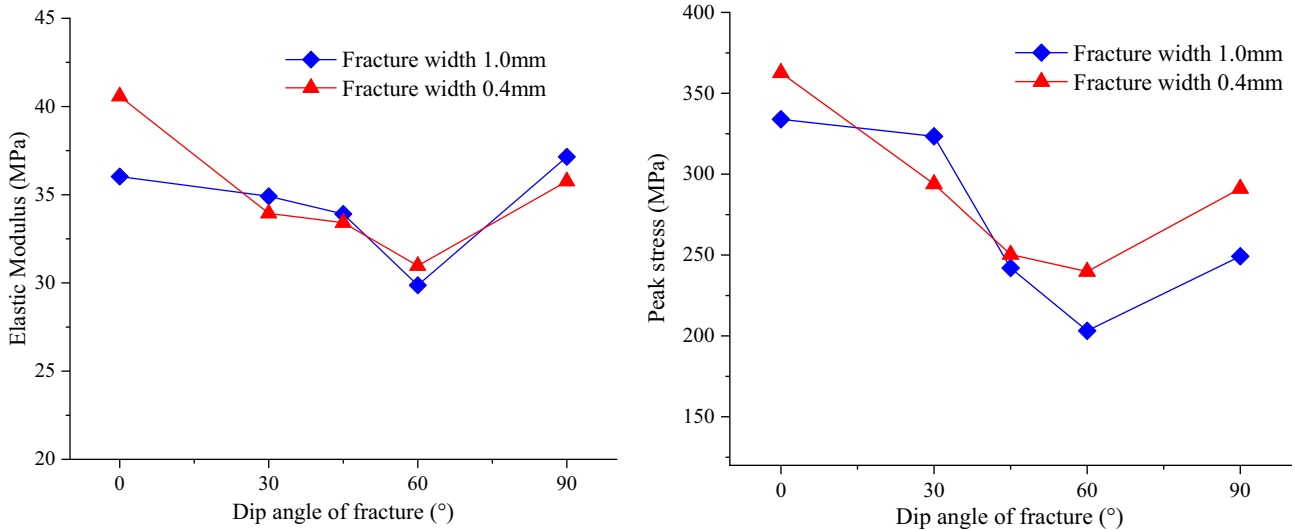


Fig. 9 Strength curves of granite with different fracture dip angles under triaxial loading

of 60°, the peak strengths drop to the lowest values, which decrease by 33.88% and 39.14%, respectively; similarly, at a fracture dip angle of 0°, the elastic moduli of rock samples with the fracture widths of 0.4 and 1 mm reach maxima of 40.18 and 38.03 MPa (some 30.71% and 31.97% below previous minima, respectively). The wider the fracture, the more significantly the peak strength and elastic modulus of rock samples reduce with increasing dip angle.

Analysis of the failure mode of fractured granite

1. The influence of the confining pressure

At a constant fracture length of 30 mm and a fracture dip angle of 60°, the failure modes of rock samples under uniaxial compression and triaxial compression with different confining pressures were obtained, as shown in Fig. 10.

Under uniaxial compression, two vertical cracks formed due to coalescence of opposite-wing cracks and wing cracks are generated after the samples are damaged, in which the opposite-wing cracks are much wider

than wing cracks. Under the influence of the friction effect at the end-faces of each specimen, an approximately conical failure appears, which indicates that the crack tip causes (in part) tension cracking. Under triaxial compression, opposite-wing cracks, and then co-planar cracks, are generated in samples along the pre-fabricated fractures. With increasing confining pressure, the included angle between the opposite-wing cracks and the vertical direction increases. On this condition, the specimens are severely damaged because the elastic strain energy stored in the specimens increases with increasing confining pressure and more energy is released when reaching the peak strength.

2. The influence of the fracture length

At a confining pressure of 40 MPa and fracture dip angle of 60°, the failure modes of granite samples with different fracture lengths under triaxial compression are as shown in Fig. 11. At a fracture length of 10 mm, only co-planar cracks are generated on the surface of the damaged samples, corresponding to single shear failure; at the fracture length of 20 mm, a single shear crack and two short opposite-wing cracks occur on the surface of the damaged samples, in which the opposite-wing cracks are connected with the co-planar cracks, so it still mainly appears as single shear failure; at the fracture length in the range of 30 to 40 mm, a co-planar crack connected with pre-fabricated fractures and two opposite-wing cracks cutting through the flank of samples appear on the surface of the damaged samples. In this case, the stress drop is found in the stress–strain curve as a response, which characterizes the moment of coalescence of opposite-wing cracks in the X-shaped

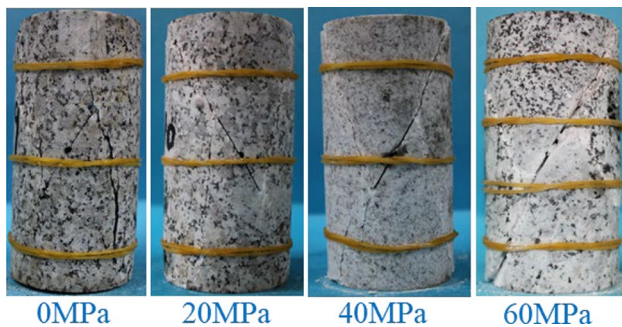
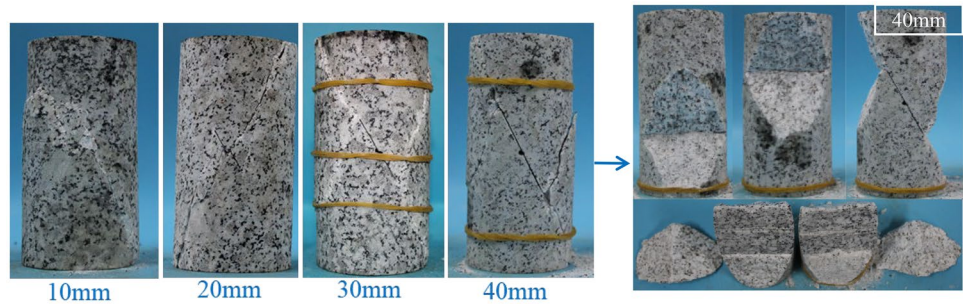


Fig. 10 Failure modes of fractured granite under triaxial loading under different confining pressures

Fig. 11 Failure modes of granite with different fracture lengths under triaxial loading



shear failure; the longer the fracture, the stronger the dominant effect of pre-fabricated fractures on the failure mode; in addition, by studying the fracture of fragments of damaged samples with a fracture length of 40 mm in the figure, it was found the fracture formed by opposite-wing cracks does not show regular corners and is significantly torn; by contrast, the fracture formed by co-planar cracks, in which the particles are crushed, is smooth and significantly sheared.

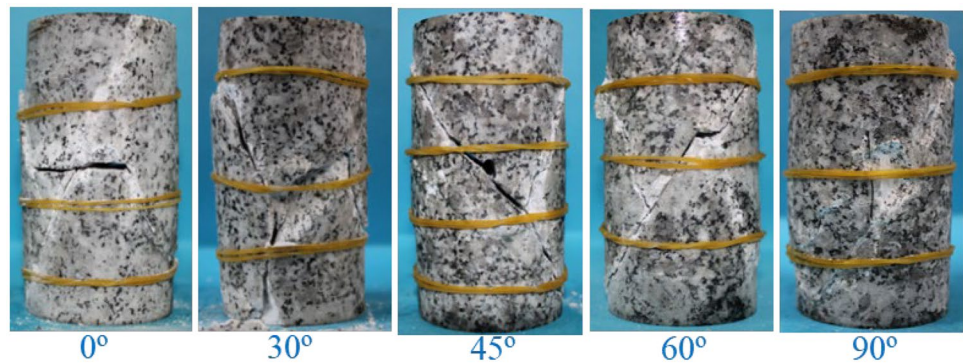
3. The influence of the fracture dip angle

At a fracture length of 30 mm and confining pressure of 40 MPa, Fig. 12 separately shows the failure modes of rock

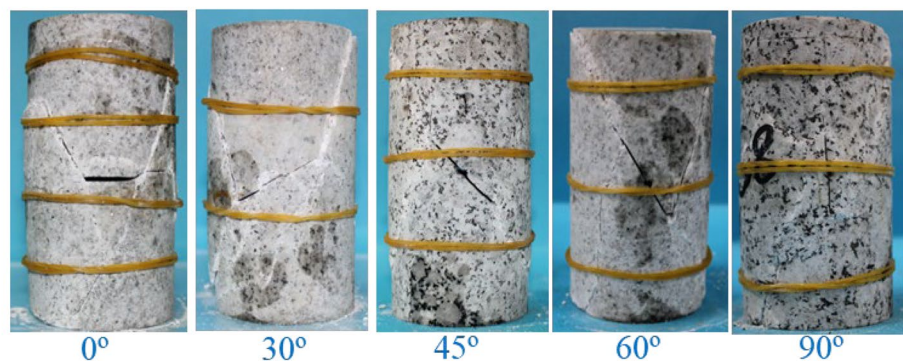
samples with different fracture dip angles at fracture widths of 0.4 and 1 mm under triaxial compression.

By comparing the failure modes of rock samples with different fracture widths, it is observed that the failure modes under the same confining pressure are similar and macroscopic fractures are more significant after the samples with a large fracture width are damaged. This is ascribed to two causes: on the one hand, the brittleness of the rock increases with the increase of the fracture width; on the other hand, due to the growth of the fracture width, a longer time is required for closure of fractures, and therefore, the samples with a large fracture width are subjected to less dissipation of energy via frictional work within the same time. As a result, more energy is used to break the rock.

Fig. 12 Typical failure modes of granite with different fracture dip angles under triaxial loading. **a** Fracture width of 1.0 mm. **b** Fracture width of 0.4 mm



(a) Fracture width of 1.0 mm



(b) Fracture width of 0.4 mm

Given fracture dip angles between 0 and 60°, the samples are globally subjected to X-shaped shear failure. To be specific, at a dip angle of 0°, a shear crack, two opposite-wing cracks, and two wing cracks are generated after samples are damaged. The shear crack passes through the center of the pre-fabricated fracture; the opposite-wing cracks propagate to co-planar shear cracks and the wing cracks run through the flank of the samples; at a dip angle of 30°, a shear crack and two opposite-wing cracks occur after samples are damaged. The shear crack goes through the center of the pre-fabricated fracture and the opposite-wing cracks run through the flank of the samples; at dip angles of 45° and 60°, a shear crack and two opposite-wing cracks separately occur on the surface of the damaged samples. The shear crack exhibits a certain angle with the pre-fabricated fracture when the dip angle of the pre-fabricated fracture is 45°, while being basically coplanar with the pre-fabricated fracture when the dip angle is 60°. The opposite-wing cracks in samples run through the flank of samples; at the dip angle of 90°, only a single shear crack is present on the surface of the damaged samples.

Energy transfer in fractured granite under triaxial loading

Theory underpinning energy calculation

Energy dissipation is regarded as an essential attribute during deformation and failure of rock, which reflects the process, whereby microdefects in rock constantly develop and rock is constantly weakened until failure. During the deformation and failure of fractured rock, energy is always exchanged with the external environment. The total energy input from the external environment is mainly transformed into the elastic strain energy and dissipated energy, which further influence the rock. The deformation characteristics of rock during energy transformation can be divided into reversible and irreversible deformations. During reversible deformation, the elastic strain energy is generated; however, energy is dissipated during the irreversible deformation in the forms of plastic deformation, damage, friction, and thermal radiation to generate the dissipated energy. Xie et al. (2005) believed that the mechanical energy input from the external environment per unit volume during the deformation of jointed rock is only transformed into elastic strain energy stored in rock and the energy dissipated during damage to the rock, that is,

$$U = U_d + U_e$$

where U , U_e , and U_d separately refer to the total strain energy (kJ/m^3) input from the external environment, the releasable elastic strain energy (kJ/m^3) stored in the rock,

and dissipated energy (kJ/m^3), which is mainly dissipated by internal damage to, and plastic deformation of, the rock.

The energy in rock specimens under triaxial compression satisfies the following relationship:

$$U = U_1 + U_3 + U_0$$

$$U_1 = \int \sigma_1 d\varepsilon_1 = \sum_{i=0}^n \frac{1}{2} (\varepsilon_{1i+1} - \varepsilon_{1i}) (\sigma_{1i+1} - \sigma_{1i})$$

$$U_3 = 2 \int \sigma_3 d\varepsilon_3 = \sum_{i=0}^n (\varepsilon_{3i+1} - \varepsilon_{3i}) (\sigma_{3i+1} - \sigma_{3i})$$

$$U_0 = \frac{3(1-2\mu)}{2E_0} \sigma_3^2$$

where U refers to the total input energy; U_1 and U_3 separately denote the axial strain energy and circumferential strain energy; U_0 is the strain energy stored in rocks under the hydrostatic stress; σ_{1i} , ε_{1i} , σ_{3i} , and ε_{3i} represent the axial stress, axial strain, circumferential stress, and circumferential strain at each point on the stress–strain curve; and E_0 and μ denote the initial elastic modulus and Poisson's ratio.

Under a triaxial state of stress, the elastic strain energy U_e at any time t satisfies the following relationship:

$$U_e = \frac{1}{2E_u^t} [\sigma_1^2 + 2\sigma_3^2 - 2\mu(2\sigma_1\sigma_3 + \sigma_3^2)]$$

where E_u^t is the elastic modulus during unloading at time t of the rock which can be replaced by the initial elastic modulus in the calculation.

Analysis of the energy transfer during the failure of fractured granite

1. The influence of the confining pressure

At a fracture length of 30 mm and a dip angle of 60°, the changes in the total energy, elastic strain energy, and dissipated energy in fractured granite during triaxial loading under different confining pressures are displayed in Fig. 13. The curves of the total energy density under different confining pressures monotonically increase on the whole; the curves of the elastic energy density increase at first and then decrease; the curves of the dissipated energy density first stabilize, and then gradually increase; without applying the confining pressure, the curves of energy density are relatively smooth, showing no residual strain energy. When applying a confining pressure, the elastic strain energy density and dissipated energy density fluctuate, and a significant residual strain

energy is stored. The greater the confining pressure on the fractured samples, the faster the growth in dissipated energy; before reaching the peak strength, the elastic strain energy is nearly equivalent to the total energy. In this stage, the damage to the samples is insignificant and the external work is mainly stored in samples in the form of elastic energy; when approaching the stress peak, damage occurs and the dissipation of energy increases, an effect that is exacerbated at the stress peak; moreover, the elastic strain energy is largely released.

The concept of the energy storage limit (that is, the maximum of the elastic strain energy density) is introduced. At a large energy storage limit, the more elastic strain energy is released, the easier various disasters such as rock bursts are induced. Therefore, using data in Fig. 14, the confining pressure effect of the energy storage limit of fractured granite under triaxial compression was evaluated. The results indicate that the energy

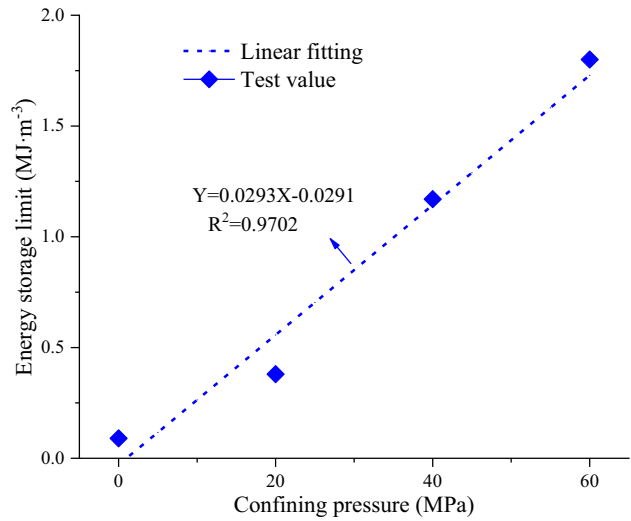
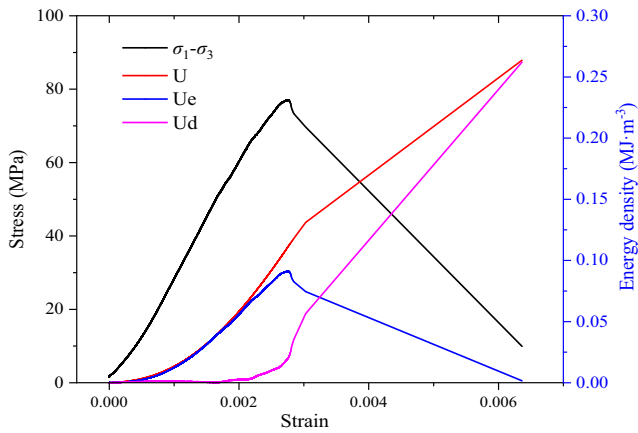
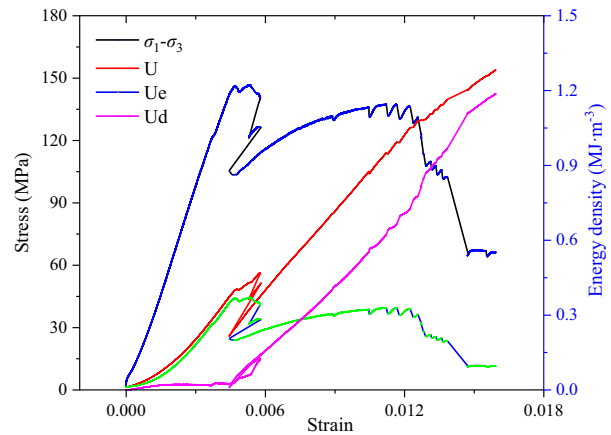


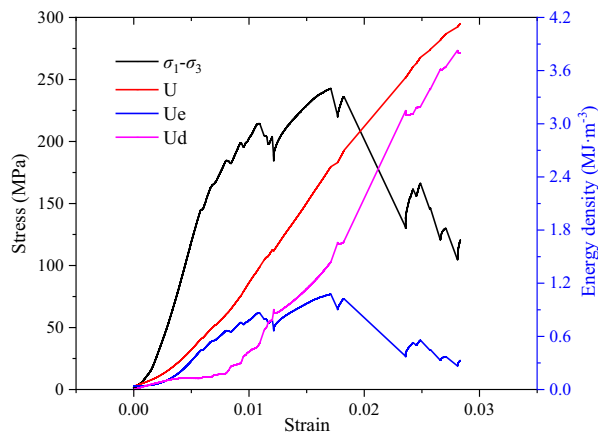
Fig. 14 Relationship between energy storage limit and confining pressure



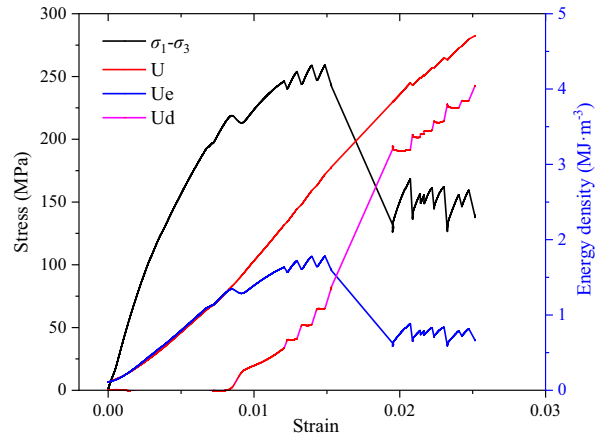
(a) Confining pressure of 0 MPa



(b) Confining pressure of 20 MPa



(c) Confining pressure of 40 MPa



(d) Confining pressure of 60 MPa

Fig. 13 Energy curve of fractured granite under triaxial loading under different confining pressures. a Confining pressure of 0 MPa. b Confining pressure of 20 MPa. c Confining pressure of 40 MPa. d Confining pressure of 60 MPa

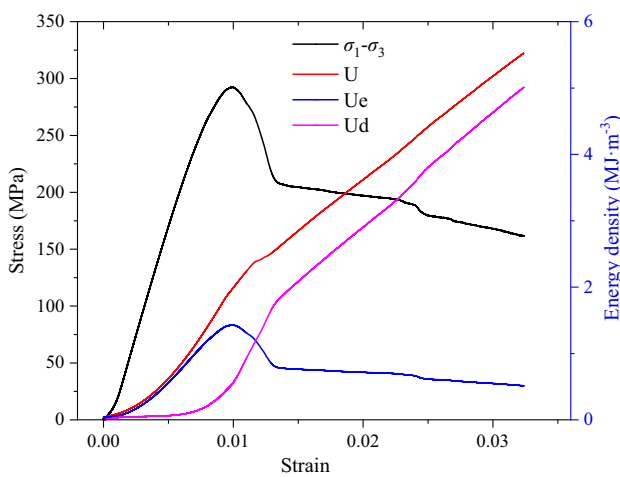
storage limit of fractured granite under triaxial compression increases linearly with the confining pressure.

2. The influence of the fracture length

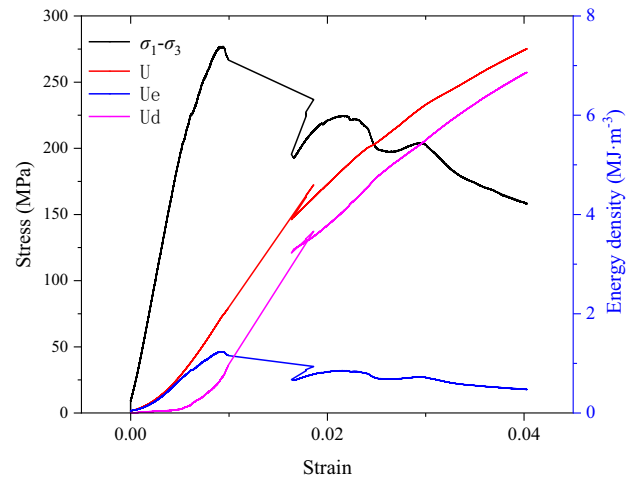
When the fracture dip angle and the confining pressure are fixed at 60° and 40 MPa separately, the change curves of the total energy, elastic strain energy, and dissipated energy in granite with different fracture lengths under triaxial loading were obtained, as shown in Fig. 15.

At a fracture length of 10 mm, the changes in energy density are relatively smooth. To be specific, the curves of the total energy density and dissipated energy density gradually increase while that of the elastic energy density first increases, and then decreases; at a fracture

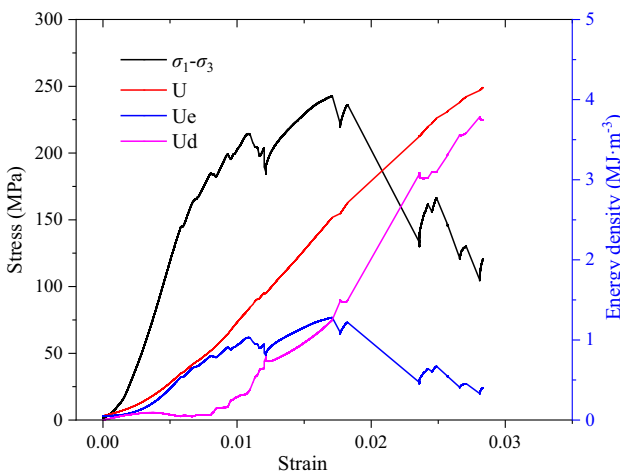
length of 20 mm, the energy density rebounds in the post-peak stage. According to the failure mode of samples, shear slip occurs in the post-peak stage and the stress fluctuates; at a fracture length of 30 mm, the total energy density continues to increase; however, the elastic strain energy density presents significant drops on three occasions: these are separately attributed to the coalescence of opposite-wing cracks; coalescence of co-planar cracks; and reduction of the post-peak friction force and cohesive force between fragments of samples. At a fracture length of 40 mm, the curve of the total energy density gradually increases and that of the elastic energy density fluctuates twice: the first event is induced by the coalescence of opposite-wing cracks; the second is triggered by the



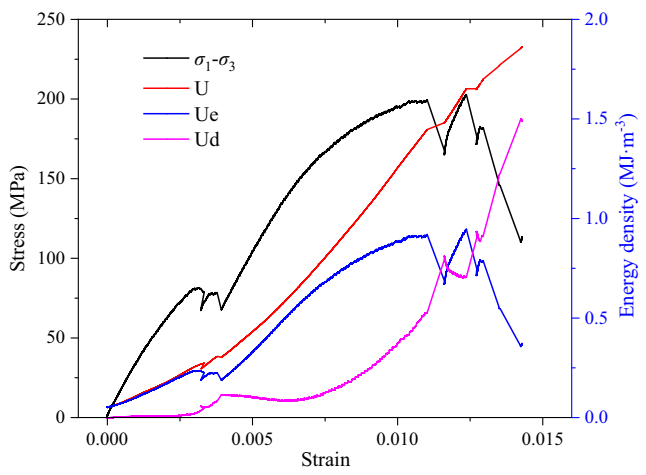
(a) Fracture length of 10 mm



(b) Fracture length of 20 mm



(c) Fracture length of 30 mm



(d) Fracture length of 40 mm

Fig. 15 Energy density evolution curve of granite with different fracture lengths under triaxial loading. **a** Fracture length of 10 mm. **b** Fracture length of 20 mm. **c** Fracture length of 30 mm. **d** Fracture length of 40 mm

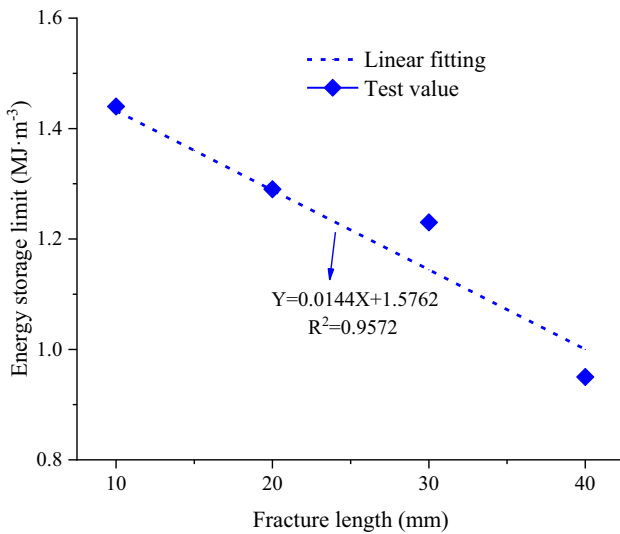


Fig. 16 Relationship between energy storage limit and crack length

rapid release of the elastic energy in the post-peak stage due to the coalescence of co-planar cracks and breaking of samples; with the growth of the fracture length, the elastic strain energy density decreases.

According to the relationship between the energy storage limit of fractured rock and the fracture length in Fig. 16, the strength and stiffness of rock decrease with increasing fracture length. Thus, even a low input energy can induce failure, implying a reduction in the energy storage limit, that is, the energy storage limit decreases linearly with the increase of the fracture length.

3. The influence of the fracture dip angle

At a fracture length at 30 mm and confining pressure at 40 MPa, the changes in the total energy, elastic strain energy, and dissipated energy in granite with different fracture dip angles under triaxial loading are displayed in Fig. 17. The triaxial loading process of granite samples

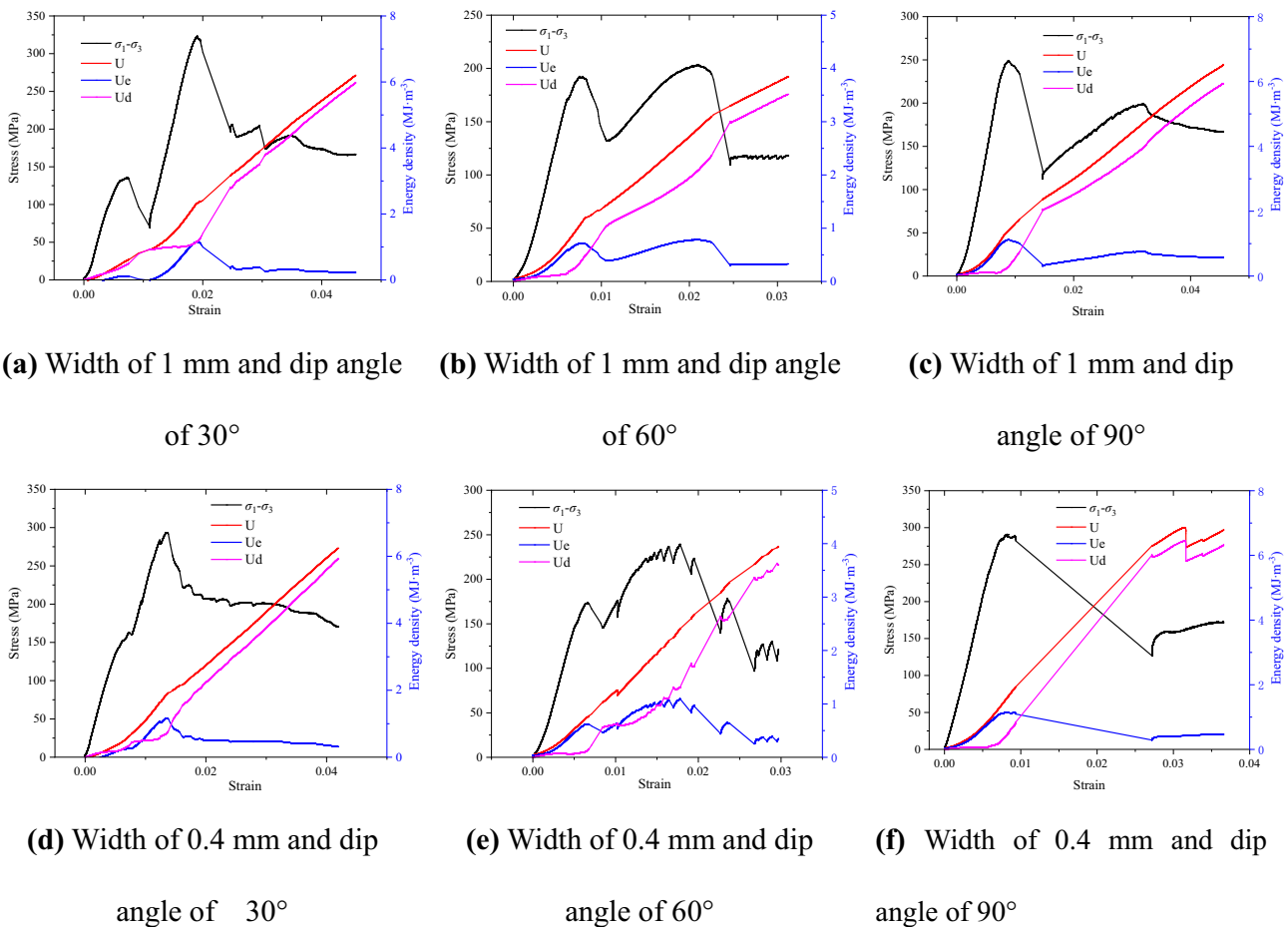


Fig. 17 Energy in granite with different fracture angles under triaxial loading. **a** Width of 1 mm and dip angle of 30°. **b** Width of 1 mm and dip angle of 60°. **c** Width of 1 mm and dip angle of 90°. **d** Width of 0.4 mm and dip angle of 30°. **e** Width of 0.4 mm and dip angle of 60°. **f** Width of 0.4 mm and dip angle of 90°

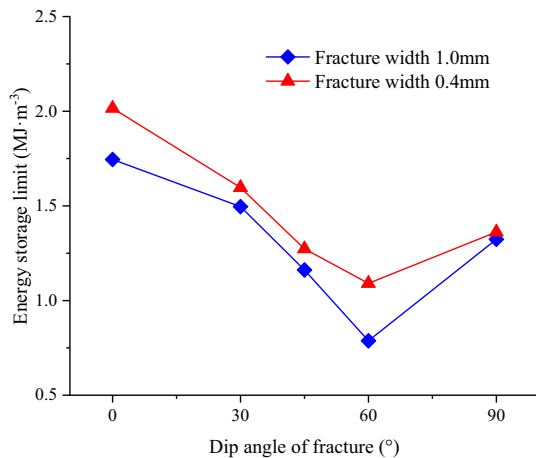


Fig. 18 Relationship between energy storage limit and fracture dip angle

with fractures can be partitioned into three stages: energy accumulation, dissipation, and release. In the loading process, the total energy density globally increases while that of the elastic strain energy density first increases, and then decreases; the dissipated energy density remains stable at first and then gradually increases. The final residual elastic energies in samples with different fracture dip angles account for similar proportions. By comparing the changes in energy density in samples with different fracture widths, it can be found that the main difference lies in the fact that the elastic strain energy density in samples with a wider fracture fluctuates to a significant extent. The peak elastic strain energy decreases with increasing fracture width. The wider the fractures, the weaker the capacity of rock to accumulate energy and the faster the release of energy; when the elastic strain energy increases most, the dissipated energy slowly increases; however, the dissipated energy greatly increases when the elastic strain energy gradually drops post-peak. This suggests that the deformation of the specimens is irreversible (post-peak) owing to crystal structures therein being severely damaged.

Figure 18 demonstrates the change in the energy storage limit of fractured granite under triaxial compression with the fracture dip angle. By comparing fractured samples with two different widths, the samples were found to have a low-energy storage limit when showing a large fracture width. The reason is that the stiffness and strength of samples decrease with the growth of the fracture width, thus reducing the energy storage limit. The energy storage limit first decreases, and then increases with increasing fracture

dip angle. At a dip angle of about 60°, the energy storage limit drops to its minimum.

Conclusions

The original rock was sampled from underground powerhouses of Shuangjiangkou Hydropower Station in southwest China to prepare the granite samples with different shapes of fractures. On this basis, the changes in the stress–strain relationship, peak strength, etc. and the energy transfer during failure of granite with different shapes of fractures under triaxial loading was obtained. The main conclusions are drawn as follows:

1. The peak strength linearly increases with the confining pressure; the peak strength under triaxial compression is much larger than that under uniaxial compression. The change of the confining pressure shows an insignificant influence on the elastic modulus; different fracture lengths exert generally coincident influences on the peak strength and on the elastic modulus: the two parameters both decrease with increasing fracture length; an increase of the fracture dip angle corresponds to the reduction at first and then growth of the peak strength and elastic modulus. The peak strength drops to a minimum at a fracture dip angle of about 60° and the wider the fracture, the more significant the change.
2. The branch cracks initiating at the crack tip mainly appear as the opposite-wing cracks, wing cracks, and co-planar cracks. The failure angle of fractured granite increases with the increase of the confining pressure; at a fracture length of about 10 mm, only co-planar cracks are generated (manifest as single shear failure). With increasing fracture length, the X-shaped shear failure predominates and the pre-fabricated fractures exert a greater influence on the failure mode; at fracture dip angles of 0 to 60°, the samples are mainly subjected to X-shaped shear failure and only single shear failure occurs at the dip angle of 90°.
3. The trend in the axial stress–strain curve of rock specimens under triaxial loading is similar to that of the elastic strain energy curve. The energy density fluctuates significantly and shows a significant residual strain energy; the energy storage limit of fractured granite linearly increases with the confining pressure and linearly decreases with increasing fracture length; moreover, the energy storage limit first decreases, and then increases as the fracture dip angle increases and decreases to its minimum at a dip angle of about 60°.

Funding This work was supported by the National Natural Science Foundation of China (Grant Nos. 51779197, 51979208), the Natural Science Foundation of Hainan Province (Grant No. 420QN291), and the Sanya Yazhou Bay Science and Technology City Administration Scientific research project (No. SKJC-KJ-2019KY02).

References

- Bobet A, Einstein HH (1998) Fracture coalescence in rock-type materials under uniaxial and biaxial compression. *Int J Rock Mech Min Sci* 35(7):863–888
- Brown ET (1949) Strength of models of rock with intermittent joints. *J Soil Mech Found Div* 96(6):1935–1949
- Du K, Li XF, Tao M, Wang SF (2020) Experimental study on acoustic emission (AE) characteristics and crack classification during rock fracture in several basic lab tests. *Int J Rock Mech Min Sci* 133:104411
- Gupta M, Alderliesten RC, Benedictus R (2015) A review of T-stress and its effects in fracture mechanics. *Eng Fract Mech* 134:218–241
- Justo J, Castro J (2021) Mechanical properties of 4 rocks at different temperatures and fracture assessment using the strain energy density criterion. *Geomech Energy Environ* 25:100212
- Li LY, Xu FG, Gao F, Wang L, Che FX (2005) Fracture mechanics analysis of rock bridge failure mechanism. *Chin J Rock Mech Eng* 24(23):4328–4334
- Li ZZ, Tao JL, Li Y (2012) Experimental Research on Acoustic Emission of Granite under Uniaxial Compression and Splitting Tensile. *Appl Mech Mater* 2047:24–27
- Liu HY (2019) Initiation mechanism of cracks of rock in compression and shear considering T-stress. *Chin J Geotech Eng* 41(7):1296–1302
- Liu MX, Liu EL (2017) Dynamic mechanical properties of artificial jointed rock samples subjected to cyclic triaxial loading. *Int J Rock Mech Min Sci* 98:54–66
- Luo Y, Wang G, Li XP, Liu TT et al (2020) Analysis of energy dissipation and crack evolution law of sandstone under impact load. *Int J Rock Mech Min Sci* 132:104359
- Mahmoud A, Mahmoud B, Raheb B (2020) Applicability of the classical fracture mechanics criteria to predict the crack propagation path in rock under compression. *Eur J Environ Civ Eng* 24(11):1761–1784
- Mishra DA, Basu A (2012) Use of the block punch test to predict the compressive and tensile strengths of rocks. *Int J Rock Mech Min Sci* 51:119–127
- Patricia R, Paola A, Tarcisio C (2016) Characterization of rock cracking patterns in diametral compression tests by acoustic emission and petrographic analysis. *Int J Rock Mech Min Sci* 83:73–85
- Rashidi MM, Ayatollahi MR, Berto F (2018) Rock fracture toughness under mode II loading: a theoretical model based on local strain energy density. *Rock Mech Rock Eng* 51:243–253
- Wang Y, Feng WK, Hu RL, Li CH (2020a) Fracture evolution and energy characteristics during marble failure under triaxial fatigue cyclic and confining pressure unloading (FC-CPU) conditions. *Rock Mech Rock Eng* 1–20
- Wang Y, Han JQ, Li CH (2020b) Acoustic emission and CT investigation on fracture evolution of granite containing two flaws subjected to freeze–thaw and cyclic uniaxial increasing-amplitude loading conditions. *Constr Build Mater* 260:119769
- Wang Y, Li CH, Han JQ (2020c) On the effect of stress amplitude on fracture and energy evolution of pre-flawed granite under uniaxial increasing-amplitude fatigue loads. *Eng Fract Mech* 240:107366
- Wang Y, Zhao QH, Xiao YG, Hou Z (2020d) Influence of time-lagged unloading paths on fracture behaviors of marble using energy analysis and post-test CT visualization. *Environ Earth Sci* 79(10):1–20
- Wu FQ, Deng Y, Wu J, Li B, Sha P, Guan SG, Zhang K, He KQ, Liu HD, Qiu SH (2020a) Stress–strain relationship in elastic stage of fractured rock mass. *Eng Geol* 268:105498
- Wu XL, Wang G, Li GX, Han W et al (2020b) Research on shear behavior and crack evolution of symmetrical discontinuous rock joints based on FEM-CZM. *Symmetry* 12(8):1314
- Xie HP, Ju Y, Li LY (2005) Criteria for strength and structural failure of rocks based on energy dissipation and energy release principles. *Chin J Rock Mech Eng* 24(17):3003–3010
- Yang J, Yang SQ, Liu GJ et al (2021) Experimental study of crack evolution in prefabricated double-fissure red sandstone based on acoustic emission location. *Geomech Geophys Geo-Energy Georesour* 7(1)
- Yang RS, Li WY, Yue ZW, Kontoni DP (2020) Comparative study on dynamic mechanical properties and energy dissipation of rocks under impact loads. *Shock Vib* 2020:1–15
- Yang SQ, Liu XR, Jing HW (2015) Experimental investigation on fracture coalescence behavior of red sandstone containing two unparallel fissures. *Int J Rock Mech Min Sci* 63(5):82–92
- Zeng W, Liu XJ, Liang LX, Zhuang DL (2019) Experimental study on the energy evolution of shales unloading failure. *Chin J Undergr Space and Eng* 15(03):719–726
- Zhang SC, Li YY, Liu H, Ma XW (2021) Experimental investigation of crack propagation behavior and failure characteristics of cement infilled rock. *Constr Build Mater* 268:121735
- Zhang W, Valliappan S (1990) Analysis of random anisotropic damage mechanics problems of rock mass. *Rock Mech Rock Eng* 23(4):91–112
- Zhang Y, Feng XT, Yang CX, Han Q, Wang ZF, Kong R (2020) Evaluation method of rock brittleness under true triaxial stress states based on pre-peak deformation characteristic and post-peak energy evolution. *Rock Mech Rock Eng* 1–15
- Zheng QS, Liu EL, Liu MX (2019) Influence of dip angle of structural planes on mechanical properties of artificial rock samples under triaxial test conditions. *Rock Soil Mech* 40(05):1854–1861
- Zheng QS, Liu EL, Sun P, Liu MX, Yu D (2020) Dynamic and damage properties of artificial jointed rock samples subjected to cyclic triaxial loading at various frequencies. *Int J Rock Mech Min Sci* 128:104243
- Zhou YQ, Sheng Q, Li NN, Fu XD (2020) Numerical analysis of the mechanical properties of rock materials under tiered and multi-level cyclic load regimes. *Soil Dyn Earthq Eng* 135:106186
- Zhu ZQ, Sheng Q, Xiao PW, Liu JG (2011) Analysis of energy dissipation in process of unloading confining pressure failure of rocks. *Chin J Rock Mech Eng* 30(S1):2675–2681